


Cross sections for neutron-induced reactions from surrogate data: Reexamining the Weisskopf-Ewing approximation for (n, n') and $(n, 2n)$ reactions

Oliver C. Gorton ^{*}*San Diego State University, San Diego, California 92182, USA*Jutta E. Escher [†]*Lawrence Livermore National Laboratory, Livermore, California 94550, USA* (Received 5 February 2021; accepted 31 March 2023; published 27 April 2023)

Background: Modeling nuclear reaction networks for nuclear science applications and for simulations of astrophysical environments relies on cross section data for a vast number of reactions, many of which have never been measured. Cross sections for neutron-induced reactions on unstable nuclei are particularly scarce, since they are the most difficult to measure. Consequently, we must rely on theoretical predictions or indirect measurements to obtain the requisite reaction data. For compound nuclear reactions, the surrogate reaction method can be used to determine many cross sections of interest.

Purpose: Earlier work has demonstrated that cross sections for neutron-induced fission and radiative neutron capture can be determined from a combination of surrogate reaction data and theory. For the fission case, it was shown that the Weisskopf-Ewing approximation, which significantly simplifies the implementation of the surrogate method, can be employed. Capture cross sections cannot be obtained, and require a detailed description of the surrogate reaction process. In this paper we examine the validity of the Weisskopf-Ewing approximation for determining unknown (n, n') and $(n, 2n)$ cross sections from surrogate data.

Methods: Using statistical reaction calculations with realistic parametrizations, we investigate first whether the assumptions underlying the Weisskopf-Ewing approximation are valid for (n, n') and $(n, 2n)$ reactions on representative target nuclei. We then produce simulated surrogate reaction data and assess the impact of applying the Weisskopf-Ewing approximation when extracting (n, n') and $(n, 2n)$ cross sections in situations where the approximation is not strictly justified.

Results: We find that peak cross sections can be estimated using the Weisskopf-Ewing approximation, but the shape of the (n, n') and $(n, 2n)$ cross sections, especially for low neutron energies, cannot be reliably determined without accounting for the angular-momentum differences between the neutron-induced and surrogate reaction.

Conclusions: To obtain reliable (n, n') and $(n, 2n)$ cross sections from surrogate reaction data, a detailed description of the surrogate reaction mechanisms is required. To do so for the compound-nucleus energies and decay channels relevant to these reactions, it becomes necessary to extend current modeling capabilities.

DOI: [10.1103/PhysRevC.107.044612](https://doi.org/10.1103/PhysRevC.107.044612)

I. BACKGROUND AND NEED

Nuclear reaction data are required for many applications in both basic and applied science, whether it be for modeling the origin of elements in the universe, the safe operation of a next-generation reactors, or for national-security applications [1,2]. Nuclear reaction libraries provide evaluated reaction data for many such applications [3]. These evaluations are based on nuclear reaction calculations anchored to experimental data and state-of-the-art nuclear theory. As many reaction cross sections of interest cannot be measured directly, due to short lifetimes or high radioactivity of the target nuclei involved, indirect methods are being developed [4–7] to address the gaps and shortcomings in present databases.

In this paper we focus on the “surrogate reaction method” [6,8], an indirect approach for determining cross sections for compound-nuclear reactions. Compound-nuclear, or “statistical,” reactions proceed through the formation of an intermediate “compound” nucleus $n + A \rightarrow B^*$, followed by a decay into reaction products $B^* \rightarrow c + C$. The appropriate formalism for calculating cross sections for these reactions is the Hauser-Feshbach formalism [9,10]. Hauser-Feshbach calculations are often quite limited in accuracy due to uncertainties in the nuclear physics inputs needed, in particular the nuclear structure inputs associated with the decay of the compound nucleus (CN).

In a surrogate reaction experiment, the CN of interest is produced via an alternative, experimentally accessible reaction, and the probability of decay into the reaction channel of interest is measured. From this data, constraints for the Hauser-Feshbach calculations can be obtained.

The surrogate method has some significant advantages over alternative indirect approaches: (1) the method does not

^{*}ogorton@sdsu.edu; University of California, Irvine, California 92679, USA.

[†]escher1@llnl.gov

require measurement of auxiliary nuclear properties that are not available for unstable nuclei and for which interpolation or extrapolation procedures are associated with uncontrolled uncertainties [14,15], and (2) The method can be used for reactions that populate energies well above particle separation thresholds in the CN, i.e., it is applicable not only to (n, γ) , but also to (n, n') , $(n, 2n)$, (n, p) , (n, f) reactions (and similarly to charged-particle-induced reactions).

Alternative indirect approaches, in particular the Oslo and β -Oslo methods [7], aim at extracting level densities and γ -ray strength functions by populating a CN below the neutron separation energy via a transfer reaction or β decay, respectively, and measuring the resulting gamma emission. To separate the level density from the γ -ray strength function, the Oslo-type analyses require the use of additional information; typically, this includes average neutron resonance spacings (D_0) and the average radiative widths, $\langle \Gamma_\gamma \rangle$. For neutron-induced reactions on unstable nuclei, however, these quantities are not available and are difficult to estimate reliably. In addition, the (n, n') and $(n, 2n)$ reactions of interest here require CN decay information for excitation energies well above the neutron separation energy.

Both the surrogate method and the Oslo/ β -Oslo methods require the calculation of the formation of the CN in the desired reaction. This involves, for neutron-induced reactions, knowledge of a neutron-nucleus optical model potential. For target nuclei near stability, global nucleon-nucleus optical models exist [16,17], which are expected to be reliable at least a few isotopes away from stability. While these optical models are often applied far from stability, little is known about how well they work in these areas of the isotopic chart [18–20]. More theoretical work is needed to develop the next generation of optical model potentials. These need to display the proper dispersive properties and reflect the correct isospin dependence, and are ideally based on microscopic theories [21–24]. In addition, new experiments at radioactive beam facilities are needed to constrain and test the optical models.

Applications of the surrogate method to (n, f) reactions have a long history [6] and in recent years scientists successfully used the approach to obtain neutron capture cross sections [14,15,25]. In this paper, we focus on possible applications to (n, n') and $(n, 2n)$ reactions.

Figure 1 illustrates how the surrogate approach can be used to determine $^{90}\text{Zr}(n, \gamma)$, $^{90}\text{Zr}(n, n')$, and $^{90}\text{Zr}(n, 2n)$ cross sections from a surrogate inelastic scattering experiment. For incident neutron energies below a few MeV, neutron capture and inelastic neutron scattering compete with each other; above $E_n \approx 10$ MeV, one- and two-neutron emission compete with each other. Proton and α emission compete only weakly and have to be accounted for, but are not shown here. In actinides, fission may compete at all energies. If the surrogate reaction measurement is designed to cover a broad energy range, it becomes possible to determine cross sections for all three neutron-induced reactions in *one* experiment. The decay channel of interest is determined either by measuring γ transitions specific to one of the three decay products, or by detecting outgoing neutrons, in coincidence with the scattered ^3He particle. Experimentalists conducting

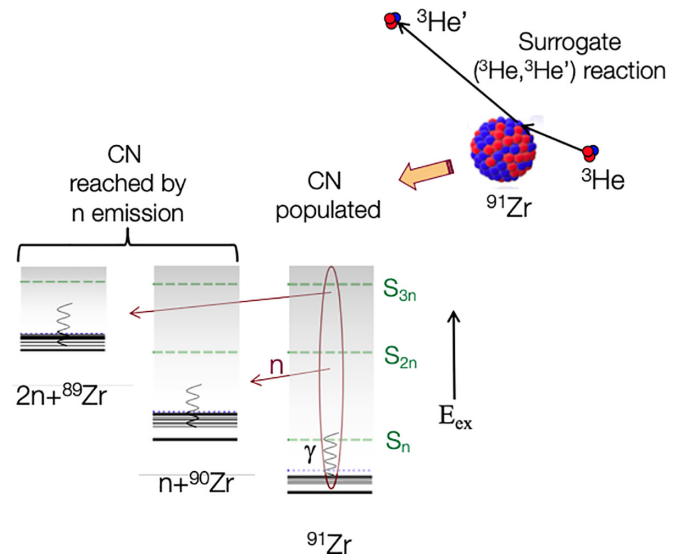


FIG. 1. Surrogate reactions approach for the simultaneous measurement of $^{90}\text{Zr}(n, \gamma)$, $^{90}\text{Zr}(n, n')$, and $^{90}\text{Zr}(n, 2n)$ cross sections. A recent inelastic scattering experiment produced the CN up to about 30 MeV, i.e., above the two-neutron threshold [11]. Subsequent decay via emission of γ 's, one neutron, and two neutrons, produces final ^{91}Zr , ^{90}Zr , and ^{89}Zr nuclei, respectively. The example here displays a situation in which discrete γ transitions between low-lying states in three nuclei are used to determine the decay channel probabilities. A complementary decay measurement that focuses on the detection of neutrons is under development as well [12]. The ^{90}Zr experiment serves as a benchmark, since multiple neutron-induced reactions for the stable ^{90}Zr nucleus are known from direct measurements [13].

these measurements have utilized discrete γ rays and are currently developing the capability to use neutron measurements.

In principle, a careful description of the surrogate reaction mechanism is required to obtain the cross section of the desired reaction. This is because one must account for the differences in the decay of the CN due to the angular-momentum and parity differences in the surrogate and desired reactions (the spin-parity mismatch). Indeed, (n, γ) reactions are very sensitive to spin effects, particularly in nuclei with low level density [26–28]. On the other hand, sensitivity studies for surrogate (n, f) applications have shown that neglecting the spin-parity mismatch yields reasonable results, except at low neutron energies [29–31]. Neglecting the spin-parity mismatch between the surrogate and desired reactions is known as the Weisskopf-Ewing approximation, and it greatly simplifies the extraction of the cross sections from surrogate data, as only a simple theoretical treatment is required.

It is the purpose of this paper to investigate what is required to determine reliable cross sections for (n, n') and $(n, 2n)$ reactions from surrogate data. Specifically, we carry out sensitivity studies that examine the validity of the Weisskopf-Ewing approximation for these two reactions for several regions of the nuclear chart.

In the next section, we review the surrogate reaction formalism and provide details on the Weisskopf-Ewing approximation. In Sec. III, we describe our procedure for testing

the assumption of the approximation, and for investigating the consequences of applying the approximation in situations where its assumptions are not strictly valid. In Sec. IV, we present results for zirconium, gadolinium and uranium nuclei, which are representative of spherical and deformed nuclei, respectively. We summarize our findings and make recommendations in Sec. V.

II. REACTION FORMALISM

Here we summarize the Hauser-Feshbach formalism for calculating the cross section of a compound-nuclear reaction and its relationship to the description of a surrogate reaction. This clarifies how surrogate reaction data can be used to constrain calculations for unknown cross sections. We outline the circumstances under which the Weisskopf-Ewing approximation can be used to simplify the analysis used to obtain the desired compound cross section.

A. Theory for the desired reaction

The Hauser-Feshbach (HF) statistical reaction formalism properly accounts for conservation of angular momentum and parity in compound-nuclear reactions. For a reaction with entrance channel $\alpha = a + A$ that forms the CN B^* , which subsequently decays into the exit channel $\chi = c + C$,

$$a + A \rightarrow B^* \rightarrow c + C,$$

the HF cross section can be written as

$$\sigma_{\alpha\chi}(E_a) = \sum_{J,\pi} \sigma_{\alpha}^{CN}(E_{ex}, J^{\pi}) G_{\chi}^{CN}(E_{ex}, J^{\pi}). \quad (1)$$

Here E_a and E_{ex} are the kinetic energies of the projectile a and the excitation energy of the compound nucleus B^* , respectively. They are related to each other via $E_a = \frac{m_A}{m_a + m_A}(E_{ex} - S_a)$, where S_a is the energy needed to separate the particle a from the nucleus B^* . m_a and m_A are the masses of the projectile and target, respectively. J and π are the spin and parity of the compound nucleus and $\sigma_{\alpha}^{CN}(E_{ex}, J^{\pi})$ is the cross section for the forming the compound nucleus B^* with spin and parity J^{π} at energy E_{ex} . The $\sigma_{\alpha}^{CN}(E_{ex}, J^{\pi})$ and their sum, the compound-formation cross section $\sigma_{\alpha}^{CN}(E_{ex}) = \sum_{J,\pi} \sigma_{\alpha}^{CN}(E_{ex}, J^{\pi})$, can be determined using an appropriate optical model for the a -nucleus interaction. Width fluctuation corrections have been omitted to simplify the notation in Eq. (1), but are included in the calculations.

$G_{\chi}^{CN}(E_{ex}, J^{\pi})$ is the probability that the CN decays via the exit channel χ . For reactions that emit one particle (neutron, proton, alpha, etc.) it depends on the convolution of the transmission coefficient $T_{\chi l_c j_c}^J$ with the level density $\rho_{j_c}(U)$ for the residual nucleus, divided by analogous terms for all competing decay modes χ' :

$$G_{\chi}^{CN}(E_{ex}, J^{\pi}) = \frac{\sum_{l_c j_c} T_{\chi l_c j_c}^J \rho_{j_c}(U) dE_{\chi}}{\sum_{\chi' l'_c j'_c} T_{\chi' l'_c j'_c}^J \rho_{j'_c}(U') dE_{\chi'}}. \quad (2)$$

The quantities l_c and l'_c are the relative orbital angular momenta in the exit channels. $\vec{j}_{\chi} = \vec{j}_c + \vec{j}_C$ is the exit channel spin, related to the total spin $\vec{J} = \vec{l}_a + \vec{j}_{\alpha} = \vec{l}_c + \vec{j}_{\chi}$ by con-

servation of momentum with the entrance channel spin, $\vec{j}_{\alpha} = \vec{j}_a + \vec{j}_A$. $\rho_C(U, j_C)$ is the density of levels of spin j_C at energy U in the residual nucleus.

Contributions from decays to discrete levels and to regions described by a level density have to be accounted for and are implicitly included in the integrals in both the numerator and denominator of Eq. (2). For reactions that involve sequential decays, e.g., the emission of two neutrons in $(n, 2n)$, Eq. (2) is repeatedly applied: first to determine the possible outcomes of the CN decay in the first step of the emission chain, and second to follow the subsequent decays of the intermediate compound nuclei created. In HF calculations, the final cross sections are obtained by tracking all possible decays in this manner. All sums over quantum numbers must respect parity conservation, although this is not explicitly expressed here.

In this paper, we focus on neutron-induced reactions, i.e., $\alpha = n + A$. For such reactions, the optical model potential, used to calculate the first factor in Eq. (1), is well approximated by a one-body potential [32]. By far the greatest source of uncertainty comes from the decay probabilities, a fact that can be attributed to uncertainties in the nuclear structure inputs. *Ab initio* shell-model calculations can provide nuclear structure information for nuclei with only a dozen or so nucleons, and traditional shell-model calculations cover a limited number of nuclei, primarily near closed shells, containing up to around 100 nucleons. Mean-field and beyond-mean field approaches cover a wider range of nuclei, but calculating the relevant structure quantities (level densities and gamma-ray strength functions) is nontrivial. While much progress has been made toward achieving microscopic nuclear structure inputs for HF calculations of medium-mass and heavy nuclei, many isotopes needed for applications and for simulating stellar environments are currently out of reach.

In the absence of microscopic predictions of structural properties, phenomenological models are used for nuclear level densities and electromagnetic transition strengths, with parameters that are fitted to available data. Much effort has been devoted to generate global or regional parameter systematics [3] that can be utilized as to perform HF calculations and build nuclear reaction evaluations [33–36]. Alternatively, it is possible to use surrogate reaction data to obtain experimental constraints on the decay probabilities.

B. Full modeling of the surrogate reaction

In a surrogate experiment, such as the one schematically shown in Fig. 1, the compound nucleus B^* is produced by an inelastic scattering or transfer reaction $d + D \rightarrow b + B^*$, and the desired decay channel is observed in coincidence with the outgoing particle b at angle θ_b .

The probability of forming B^* in the surrogate reaction (with specific values for E_{ex} , J , π) is $F_{\delta}^{CN}(E_{ex}, J, \pi, \theta_b)$, where δ refers to the surrogate reaction $d + D \rightarrow b + B^*$. The quantity

$$P_{\delta\chi}(E_{ex}, \theta_b) = \sum_{J,\pi} F_{\delta}^{CN}(E_{ex}, J^{\pi}, \theta_b) G_{\chi}^{CN}(E_{ex}, J^{\pi}), \quad (3)$$

which gives the probability that the CN B^* was formed with energy E_{ex} and decayed into channel χ , can be obtained

experimentally by detecting a discrete γ -ray transition characteristic of the residual nucleus (or some other suitable observable).

The distribution $F_{\delta}^{CN}(E_{ex}, J, \pi, \theta_b)$, which may be very different from the CN spin-parity populations following the absorption of a neutron in the desired reaction, has to be determined theoretically, so that the branching ratios $G_{\chi}^{CN}(E_{ex}, J^{\pi})$ can be extracted from the measurements.

In practice, the decay of the CN is modeled using a Hauser-Feshbach-type decay model and the $G_{\chi}^{CN}(E_{ex}, J^{\pi})$ are obtained by adjusting parameters in the model to reproduce the measured probabilities $P_{\delta\chi}(E_{ex}, \theta_b)$. Subsequently, the sought-after cross section for the desired (neutron-induced) reaction can be obtained by combining the calculated cross sections $\sigma_{n+A}^{CN}(E_{ex}, J^{\pi})$ for the formation of B^* (from $n+A$) with the extracted decay probabilities $G_{\chi}^{CN}(E_{ex}, J^{\pi})$; see Eq. (1). Modeling the CN decay begins with an initial (“prior”) description of structural properties of the reaction products (level densities, branching ratios, internal conversion rates), plus a fission model for cases which involve that decay mode. Finally, a procedure for fitting the parameters of the decay models, e.g., via a Bayesian approach as introduced in Ref. [14], needs to be implemented to determine the desired cross section, along with uncertainties.

This procedure was recently employed to determine cross sections for neutron capture on the stable ^{90}Zr and ^{95}Mo isotopes (for benchmark purposes), as well as for neutron capture on the unstable ^{87}Y nucleus [14,15]. It was also used to simultaneously infer the (n, γ) and low-energy (n, f) cross sections for ^{239}Pu [25].

Such a full treatment of a surrogate experiment is challenging: It involves taking into account differences in the angular momentum J and parity π distributions between the compound nuclei produced in the desired and surrogate reactions, as well as their effect on the decay of the compound nucleus. Predicting the spin-parity distribution $F_{\delta}^{CN}(E_{ex}, J, \pi, \theta_b)$ resulting from a surrogate reaction is a nontrivial task since a proper treatment of direct reactions leading to highly excited states in the intermediate nucleus B^* involves a description of particle transfers, and inelastic scattering, to unbound states. In addition, a complete treatment should include consideration of width fluctuation corrections and the possible decay prior to reaching equilibrium.

For capture cross sections, it was shown that this type of approach is needed to account for the spin-parity mismatch in the surrogate experiment [26,27], while for fission applications it often suffices to employ the much simpler Weisskopf-Ewing or ratio approximations [31].

C. Weisskopf-Ewing approximation for neutron-nucleus reactions and surrogate coincidence probabilities

The Hauser-Feshbach expression for the cross section of the desired neutron-induced reaction, Eq. (1), conserves total angular momentum J and parity π . Under certain conditions the branching ratios $G_{\chi}^{CN}(E_{ex}, J^{\pi})$ can be treated as independent of J and π , and the cross section for the desired reaction

simplifies to

$$\sigma_{n+A, \chi}^{WE}(E_{ex}) = \sigma_{n+A}^{CN}(E_{ex}) \mathcal{G}_{\chi}^{CN}(E_{ex}), \quad (4)$$

where $\sigma_{n+A}^{CN}(E_{ex}) = \sum_{J\pi} \sigma_{n+A}^{CN}(E_{ex}, J^{\pi})$ is the cross section describing the formation of the compound nucleus at energy E_{ex} , and $\mathcal{G}_{\chi}^{CN}(E_{ex})$ denotes the $J\pi$ -independent branching ratio for the exit channel χ . This is the Weisskopf-Ewing limit of the Hauser-Feshbach theory [32].

The Weisskopf-Ewing limit provides a simple and powerful approximate way of calculating cross sections for compound-nucleus reactions. In the context of surrogate reactions, it greatly simplifies the application of the method. In Sec. II B we described the process required to obtain the $J\pi$ -dependent branching ratios G_{χ}^{CN} from measurements of $P_{\delta\chi}(E_{ex})$. In the Weisskopf-Ewing limit, and because $\sum_{J\pi} F_{\delta}^{CN}(E_{ex}, J^{\pi}) = 1$,

$$P_{\delta\chi}(E_{ex}) = \mathcal{G}_{\chi}^{CN}(E_{ex}). \quad (5)$$

Calculating the direct-reaction probabilities $F_{\delta}^{CN}(E_{ex}, J, \pi, \theta_b)$ and modeling the decay of the compound nucleus are no longer required in this approximation. [In actual applications, experimental efficiencies have to be included when determining $P_{\delta\chi}(E_{ex})$; these are omitted for simplicity here, but are accounted for in the analysis of surrogate experiments.]

The conditions under which the approximate expressions (4) and (5) are obtained from Eqs. (1) and (3) are discussed in the Appendix.

In addition, the Weisskopf-Ewing approximation can be used in situations in which the surrogate reaction produces a spin distribution that is very similar to that of the desired reaction, i.e.,

$$F_{\delta}^{CN}(E_{ex}, J^{\pi}) \approx F_{n+A}^{CN}(E_{ex}, J^{\pi}), \quad (6)$$

where

$$F_{n+A}^{CN}(E_{ex}, J^{\pi}) \equiv \frac{\sigma_{n+A}^{CN}(E_{ex}, J^{\pi})}{\sum_{J\pi} \sigma_{n+A}^{CN}(E_{ex}, J^{\pi})}, \quad (7)$$

since the weighting of the J^{π} -dependent decay probabilities in the measured $P_{\delta\chi}(E_{ex})$ is the same as the weighting relevant to the desired reaction. While some intuitive arguments have been forwarded in favor of specific surrogate reaction mechanisms that might satisfy the condition (6), not much is actually known about what spin-parity distributions F_{δ}^{CN} are obtained when producing a CN at high excitation energies ($E_{ex} > 5$ MeV) via inelastic scattering or a transfer reaction. We therefore investigate both the dependence of realistic decay probabilities $G_{\chi}^{CN}(E_{ex}, J^{\pi})$ on spin and parity (Sec. III A) and the impact of using the Weisskopf-Ewing approximation in situations in which $G_{\chi}^{CN}(E_{ex}, J^{\pi})$ depends on spin and parity (Sec. III B).

III. ASSESSING THE VALIDITY OF THE WEISSKOPF-EWING APPROXIMATION

As discussed in the previous section, there are two scenarios in which it is clearly valid to employ the Weisskopf-Ewing approximation in the analysis of a surrogate experiment:

(a) The decay probabilities $G_{\chi}^{CN}(E_{ex}, J^{\pi})$ are independent of $J\pi$ for the decay channel χ of interest; or (b) The surrogate and desired reactions produce identical spin distributions (“serendipitous” or “matching” approach [6]). In addition, there are some intermediate situations in which a Weisskopf-Ewing analysis can give a good approximation to the true cross section. For instance, it is possible that the decay probabilities $G_{\chi}^{CN}(E_{ex}, J^{\pi})$ are only moderately sensitive to $J\pi$, and that the surrogate and desired reactions populate somewhat similar compound nucleus spins and parities, so that violations of the Weisskopf-Ewing limit may have little impact on the extracted cross section. Investigations into the possibility of using the Weisskopf-Ewing approximation must therefore consider *both* the behavior of the decay probabilities $G_{\chi}^{CN}(E_{ex}, J^{\pi})$ for the decay channel χ of interest *and* their influence in typical surrogate reaction analyses.

Earlier studies, which have done that, demonstrated that it is not *a priori* clear whether the Weisskopf-Ewing limit applies to a particular reaction in a given energy regime [26–28,31]. For fission applications, it was found that using the Weisskopf-Ewing approximation gives reasonable cross sections, with violations of the Weisskopf-Ewing limit occurring primarily at low energies (E_n below 1–2 MeV) and at the onset of first- and second-chance fission [31]. For neutron capture reactions, however, the $G_{\gamma}^{CN}(E_{ex}, J^{\pi})$ were found to be very sensitive to the $J\pi$ and no circumstances have been identified so far in which the Weisskopf-Ewing limit can be used to obtain capture cross sections [27].

In the present study we focus on the proposed use of the surrogate method to determine (n, n') and $(n, 2n)$ cross sections. To study the validity of the Weisskopf-Ewing approximation, we proceed in two steps:

- (1) Investigation of the $J\pi$ dependence of the decay probabilities $G_{\chi}^{CN}(E_{ex}, J^{\pi})$ for $\chi = 1n$ and $2n$, i.e., for one- and two-neutron emission.
- (2) Assessment of the impact of the $J\pi$ dependence of the $G_{\chi}^{CN}(E_{ex}, J^{\pi})$ on cross sections extracted by using the Weisskopf-Ewing approximation.

A. Method for determining spin-parity dependence

In the first step, we obtain the $G_{\chi}^{CN}(E_{ex}, J^{\pi})$ from well-calibrated Hauser-Feshbach calculations that involve the relevant decay channels. We selected $n + {}^{90}\text{Zr}$, $n + {}^{157}\text{Gd}$, and $n + {}^{238}\text{U}$ as representative cases for neutron reactions on spherical and deformed nuclei, with the uranium case representing a nucleus for which fission competes with particle evaporation and γ emission.

For each nucleus, we carried out a full Hauser-Feshbach calculation of the neutron-induced reaction and calibrated the model parameters to give an overall good fit of the known neutron cross sections. This local optimization of model parameters allows us to isolate the spin-parity effects from model uncertainties. Our optimization procedure accounted for preequilibrium effects using the two-exciton model [37], and other competing decay channels. This is necessary to accurately and realistically reproduce the data without biasing the model-space parameters. In contrast, the calculations

described in this and the following section include only contributions from compound nucleus decay. This is consistent with the goal of investigating the ability to determine the compound cross section from a Weisskopf-Ewing analysis of surrogate data.

The calculations were carried out with Hauser-Feshbach codes STAPRE [38] and YAHFC-MC [35]. The results discussed here are obtained using the latter. We extracted the branching ratios $G_{xn}^{CN}(E, J^{\pi})$ for one- and two-neutron emission ($x = 1$ and 2 , respectively) for a range of spin and parity values of the initially formed compound nuclei ${}^{91}\text{Zr}^*$, ${}^{158}\text{Gd}^*$, and ${}^{238}\text{U}^*$, and investigated their behavior as a function of the excitation energy E_{ex} of the CN. Our findings are discussed in Sec. IV A.

B. Method for demonstrating impact of spin-parity dependence

In the second step, we employ the decay probabilities $G_{xn}^{CN}(E_{ex}, J^{\pi})$ extracted above to simulate the results of possible surrogate measurements. This is done by calculating the coincidence probabilities given by Eq. (3), which are ordinarily measured in a surrogate experiment, by multiplying the $G_{xn}^{CN}(E_{ex}, J^{\pi})$ with several schematic spin-parity distributions $F_{\delta}^{CN}(E_{ex}, J^{\pi})$, summed over all relevant spins and parities:

$$P_{xn}^{\text{sim}}(E_{ex}) = \sum_{J\pi} F_{\delta}^{CN}(E_{ex}, J^{\pi}) G_{xn}^{CN}(E_{ex}, J^{\pi}). \quad (8)$$

We normalized the distributions $\sum_{J\pi} F_{\delta}^{CN}(E_{ex}, J^{\pi}) = 1$ and did not consider angle dependencies. Multiplication of these simulated coincidence probabilities $P_{xn}^{\text{sim}}(E_{ex})$ by the CN-formation cross section $\sigma_{n+A}^{CN}(E_{ex})$ then yields cross sections $\sigma_{(n,n')}^{WE}(E_n)$ and $\sigma_{(n,2n)}^{WE}(E_n)$ that correspond to a Weisskopf-Ewing analysis of the simulated surrogate measurement:

$$\sigma_{(n,xn)}^{WE}(E_n) = \sigma_{n+A}^{CN}(E_{ex}) P_{xn}^{\text{sim}}(E_{ex}) \quad (9)$$

for $x = 1, 2$. In Sec. IV B, we compare the so extracted cross sections for various spin-parity distributions F_{δ}^{CN} to each other and to the known desired cross sections.

To select relevant $J\pi$ distributions for our study, we briefly summarize what is known about $J\pi$ distributions that typically occur in neutron-induced as well as surrogate reactions.

1. Spin-parity distributions in neutron-induced reactions.

Figure 2 shows spin-parity distributions relevant to neutron-induced reactions, as predicted by calculating the compound-formation cross sections for various spins and parities, at the energies indicated. For Zr, a spherical optical-model calculation is sufficient, while rare earths and actinides require coupled-channels treatments, which can be carried out by suitably deforming a spherical optical model (see Refs. [39,40]) or by using a coupled-channels scheme that is specifically adjusted for the nucleus or nuclear region of interest (see Refs. [27,41–44]). We have used the Koning-Delaroche optical model [16] for Zr and Gd, and Soukhovitskii [41,42] for the U.

For the (n, n') and $(n, 2n)$ applications considered here, neutron energies between about 5 and 20 MeV are relevant. The examples selected here involve target nuclei with low

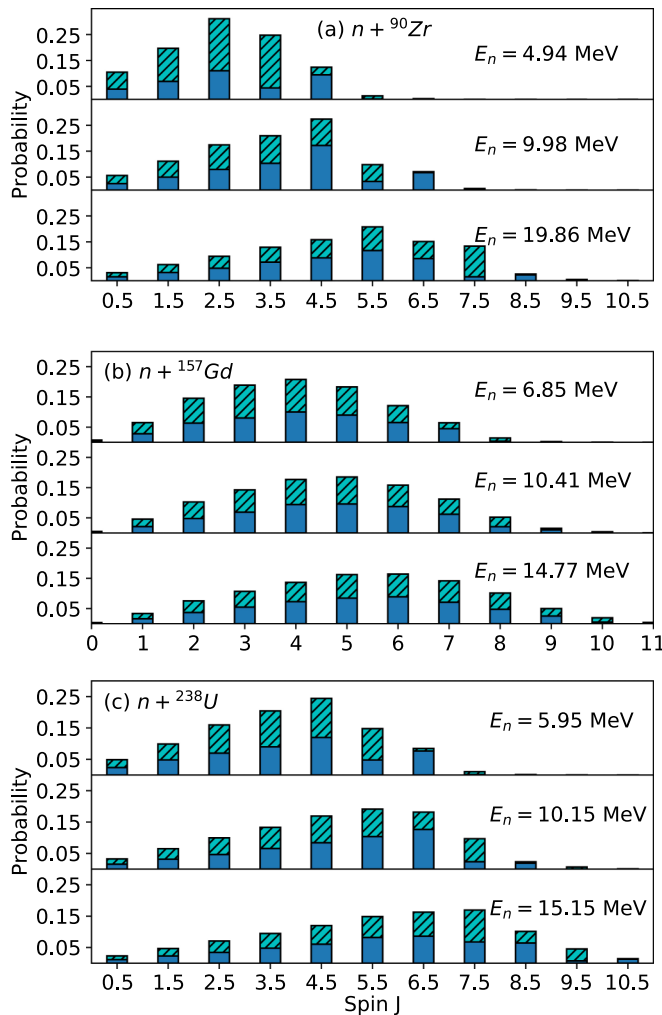


FIG. 2. Spin-parity distributions for compound nuclei produced in neutron-induced reactions, for several neutron energies E_n . Solid blue bars are positive- and hatched bars are negative-parity probabilities. Panels (b) $n + {}^{157}\text{Gd}$ and (c) $n + {}^{238}\text{U}$ are representative of deformed rare-earth and actinide nuclei, respectively, while panel (a) presents the case of a near-closed-shell nucleus, $n + {}^{90}\text{Zr}$. Neutron energies below 1 MeV are important for neutron capture reactions [27]. For the (n, n') and $(n, 2n)$ applications considered in this paper, neutron energies between about 5 and 20 MeV are relevant.

spins ($3/2^-$ for ${}^{157}\text{Gd}$ and 0^+ for the even-even ${}^{90}\text{Zr}$ and ${}^{238}\text{U}$ nuclei), so the spin-distributions are closely connected to the angular-momentum transferred in the reaction.

Panel (a) shows the population of positive and negative parity states for the $n + {}^{90}\text{Zr}$ example, for several neutron energies E_n . At $E_n \approx 1$ MeV, p -wave capture dominates [28] and produces a distribution that favors negative-parity states within a narrow range of spins. As the energy increases, contributions from higher partial waves result in smoother distributions, centered at larger angular momentum values, and with a more equal partition between positive and negative spins.

Panels (b), for $n + {}^{157}\text{Gd}$, and (c), for $n + {}^{238}\text{U}$, are representative of the situations one encounters for deformed

rare-earth and actinide nuclei, respectively. Overall, the distributions are smoother for the deformed nuclei than for the Zr case and involve larger values of angular momentum. With increasing E_n , the positive and negative parity distributions become similar, while at low energies, $E_n < 1$ MeV, the distributions can look quite different from each other [27].

2. Spin-parity distributions in surrogate reactions.

The findings of the following illustrate that it is *not* correct to assume that the spin-parity distribution of a compound nucleus produced in a surrogate reaction is given by the spin and parity behavior of the level density for that nucleus. The reaction mechanism plays a critical role in selecting which states act as doorways into the compound nucleus. The population of these doorway states determines the $J\pi$ distribution for the surrogate reaction.

Figure 1 illustrates schematically the excitation energies that a surrogate reaction has to populate in order to produce decay information relevant to (n, γ) , (n, n') , and $(n, 2n)$ reactions. For neutron capture, E_{ex} values between about 5 and 10 MeV have to be reached, for inelastic scattering, energies between approximately 10 and 20 MeV are relevant, and for $(n, 2n)$ reactions, $E_{ex} = 20\text{--}30$ MeV are important. These energy regimes exhibit high level densities, and transfer reactions aiming to populate these energy ranges are very different from those used for traditional nuclear structure studies. It should therefore not surprise that standard DWBA or even coupled-channels calculations cannot be used to reliably calculate the direct (surrogate) reactions that produce such states.

Predicting the spin-parity distributions for these higher excitation energies requires taking into account both the surrogate reaction mechanism and the nuclear structure at these higher energies. For instance, to calculate the $J\pi$ population in the compound nucleus ${}^{91}\text{Zr}^*$ that was produced via the ${}^{92}\text{Zr}(p, d)$ pickup reaction in a recent surrogate experiment with $E_p = 28.5$ MeV [14], it was necessary to consider the structure of deep neutron hole states, which exhibit considerable spreading [6,45]. Furthermore, two-step mechanisms involving $(p, d')(d', d)$ and $(p, p')(p', d)$ combinations of inelastic scattering and pickup contribute significantly to the reaction. These have a strong influence on the final spin-parity distribution in ${}^{91}\text{Zr}^*$ [14], which is shown for $E_{ex} = 7.25$ MeV in Fig. 3(a). The influence of the reaction mechanism is reflected in the differences between the predicted spin-parity population (bars) and the spin distribution in a representative level density model at the same excitation energy (green curve).

Around the neutron separation energy, i.e., in the energy region of interest to neutron capture, the angular behavior of the (p, d) cross section was found to be fairly structureless, and the $J\pi$ distribution was seen to vary little over several MeV around $E_{ex} = S_n({}^{91}\text{Zr}) = 7.195$ MeV [46]. These observations reflect the fact that the surrogate reaction does not produce a simple single-particle excitation, but populates specific doorway states which mix with neighboring complex many-body states to form the compound nucleus.

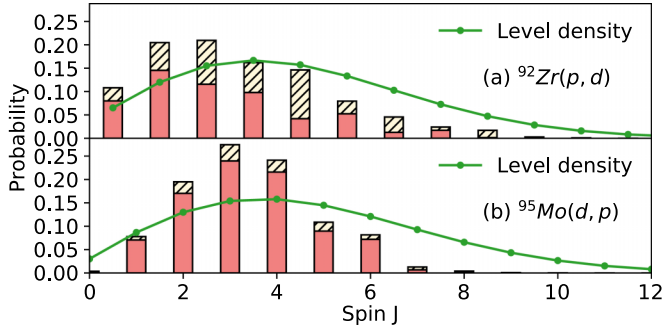


FIG. 3. Spin-parity distributions (bars) near the neutron separation energy, as predicted for use with specific surrogate experiments. Solid bars are positive-parity and hatched bars are negative-parity probabilities. Panel (a) shows the half-integer J distribution in the compound nucleus $^{91}\text{Zr}^*$ resulting from a $^{92}\text{Zr}(p, d)$ reaction with $E_p = 28.5$ MeV at $E_{ex} = 7.25$ MeV [14]. Panel (b) shows the integer valued result for $^{95}\text{Mo}(d, p)$ surrogate reaction with $E_d = 12.4$ MeV at $E_{ex} = 9.18$ MeV [15]. In both cases, the predicted spin-parity distributions were used in combination with models for the decay of the respective compound nuclei, leading to the successful determination of (benchmark) neutron capture cross sections. For comparison, the spin distribution calculated from an energy-dependent level density model, which assumes equal parity distribution, is given by the green solid curve [59].

The (d, p) transfer reaction, which at first glance seems to be a well-matched surrogate for neutron-induced reactions, turns out to involve nontrivial reaction mechanisms as well. The case of interest is that in which the deuteron breaks up in the combined Coulomb-plus-nuclear field, and the neutron is absorbed while the proton escapes and is observed in a charged-particle detector. Calculating the resulting compound nucleus $J\pi$ distribution requires a theoretical description that separates elastic from nonelastic breakup and, in principle, one also needs to separate out inelastic breakup, rearrangement, and absorption. This challenge has generated strong interest in developing a more detailed formalism for inclusive (d, p) reactions [47–51]. This formalism was used to calculate the $J\pi$ distribution relevant to the $^{95}\text{Mo}(d, p)$ surrogate reaction described in Ref. [15]. The calculated $J\pi$ distribution, for excitation energies near the neutron separation energy in ^{95}Mo is shown in Fig. 3(b). Here, again, the predicted spin-parity distribution (bars) does not follow the distribution of spins that are expected to be available at this energy, based on a representative level density model (green curve).

Inelastic scattering with charged light ions is a third type of reaction that has been employed in surrogate reaction measurements [25,52–55]. From these experiments, as well as from traditional studies of giant resonances [56–58], it is known that inelastic scattering can produce a compound nucleus at a wide range of excitation energies. There is evidence that this type of reaction is also likely to produce $J\pi$ distributions that are broad and may be centered at angular momentum values of 5–10 \hbar [25,52]. Furthermore, for inelastic α scattering, a staggering of even and odd parity populations is expected, since the reaction populates predominantly natural-parity states.

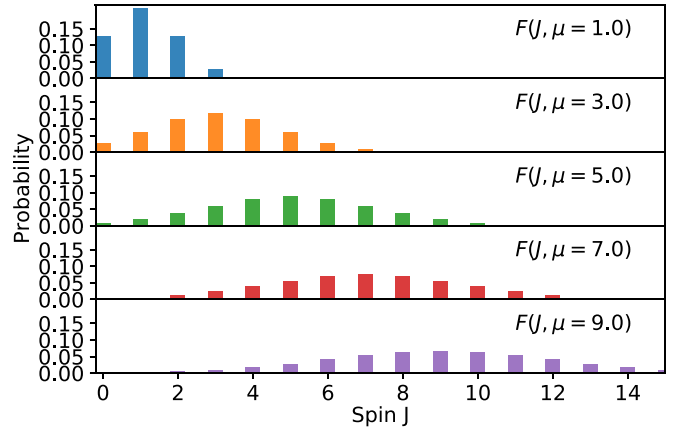


FIG. 4. Schematic spin distributions employed in the current study. Each is of the form $F(J, \mu) \propto \mathcal{N}(m = \mu, sd = \sqrt{\mu})$, where \mathcal{N} is a normal distribution and mean spin μ is indicated in the legend. The spin values J are either integer or half-integer, for even- A and odd- A nuclei, respectively, and equal probability is assigned to positive and negative parity states.

3. Schematic spin-parity distributions

In order to investigate the impact of a spin-parity mismatch between the desired and surrogate reaction on the cross section obtained from a Weisskopf-Ewing analysis, we employ the schematic distributions $F_{\delta}^{CN}(J^{\pi})$ shown in Fig. 4. We include distributions that are centered at both low and high angular-momentum values and allow for more spread-out distributions in the latter case. The distributions centered at low J values allow us to investigate situations in which the surrogate reaction populates lower spins than the desired reaction. Variations in parity are not explicitly considered for this part of the sensitivity study, as we found the decay probabilities to be less sensitive to parity than to variations in spin.

The distributions shown will be combined with the decay probabilities $G_{\chi}^{CN}(E_{ex}, J^{\pi})$ extracted from our calibrated Hauser-Feshbach calculations (see Sec. IV A) to simulate a range of possible surrogate data $P_{\delta\chi}(E_{ex}, \theta)$ using Eq. (3). For simplicity, we will neglect the energy dependence of the $J\pi$ distributions. This should be a reasonable approach for our sensitivity studies, as recent results indicate that these distributions vary slowly with energy [14,15].

IV. RESULTS

We first demonstrate that the one- and two-neutron decay probabilities depend on the spin, and to a lesser extent, the parity of the compound nucleus. The dependence is strongest at low energies and for spherical nuclei, and lesser at higher energies and for deformed nuclei. Then, we show the impact of the Weisskopf-Ewing approximation on the outcome of simulated surrogate experiments, giving insight into the effect that the spin dependence has on predicted cross sections.

A. Decay probabilities for representative nuclei

$G_{xn}^{CN}(E_{ex}, J^{\pi})$ for one- and two-neutron emission from the compound nucleus $^{91}\text{Zr}^*$ are shown in Fig. 5, for both positive

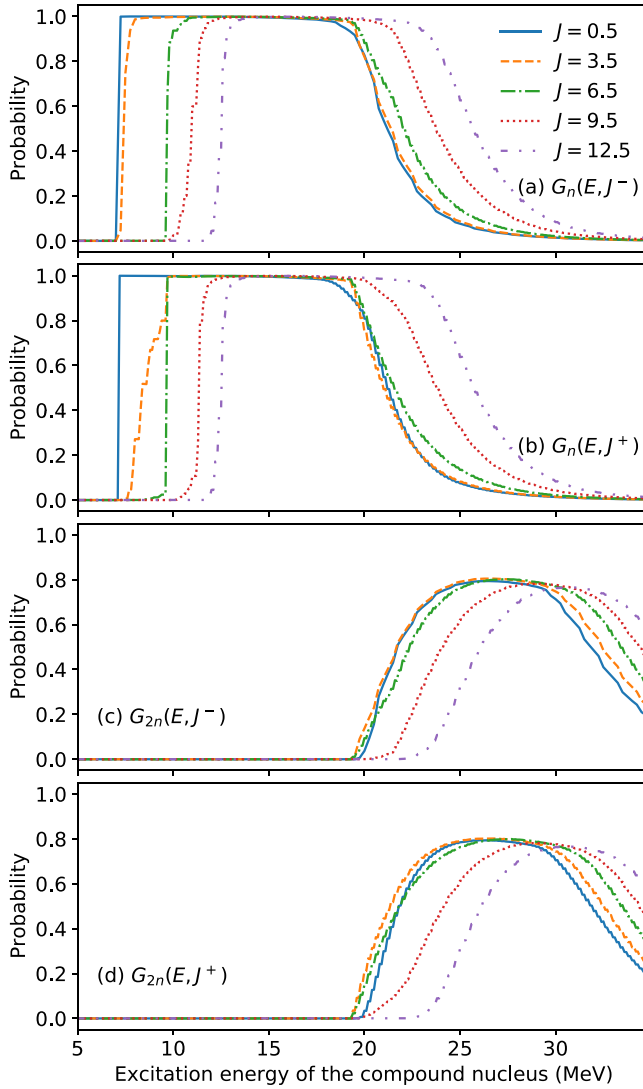


FIG. 5. Probabilities for neutron emission from the $^{91}\text{Zr}^*$ nucleus, as function of excitation energy, for various $J\pi$ values of the compound nucleus. Both decay channels exhibit a strong dependence on the spin of the compound nucleus. The variance is seen to be greatest at the onset of one-neutron emission, near $E_{ex} = S_n(^{91}\text{Zr}) = 7.194$ MeV.

and negative parities and a variety of spins. The behavior of $G_{xn}^{CN}(E_{ex}, J^\pi)$ just above the CN separation energy, corresponding to $E_{ex} = S_n(^{91}\text{Zr}) = 7.194$ MeV, is governed by the interplay of the neutron-transmission coefficients and the low-energy structure of the residual nucleus ^{90}Zr which is reached by one-neutron emission. The situation is schematically illustrated in Fig. 1. Due to the shell structure of the nucleus, the low-energy spectrum of ^{90}Zr is very sparse, with the first excited state occurring at 1.76 MeV. Since both the ground state and the first excited state have $J^\pi = 0^+$ and s - and p -wave neutron emission dominates at low energies, the residual nucleus can only be reached from low-spin states in the compound nucleus $^{91}\text{Zr}^*$. This suppression of neutron emission from all but the lowest spin states in $^{91}\text{Zr}^*$ is well

known from earlier studies of neutron capture reactions, and a dependence on parity is observed as well [6,28,60].

As the excitation energy in $^{91}\text{Zr}^*$ increases, additional states in the residual nucleus become accessible and the decay probabilities $G_{xn}^{CN}(E_{ex}, J^\pi)$ for higher J values take on nonzero values. In the region between $E_{ex} = 15$ –20 MeV, the one-neutron emission probability is essentially unity, because of the weakness of competing decay channels.

In the energy region between 20 and 27 MeV, we observe the transition from predominantly one-neutron emission to two-neutron emission. We see significant dependence of the branching ratio on the spins of the compound nucleus for $J \geq 6.5$, while there is much weaker dependence for $J \leq 6.5$. The decay probabilities are not very sensitive to parity. Figure 6 shows the analogous one- and two-neutron emission probabilities for the decay of the rare-earth nucleus ^{158}Gd . Here, the dependence on spin is weaker than in the Zr case, especially near the one-neutron separation energy of the compound nucleus. This is primarily due to the significantly higher level density in the gadolinium nuclei: While the first excited state in ^{90}Zr is at 1.76 MeV, there are 15 levels below 0.5 MeV in ^{157}Gd . In general, the level densities in deformed nuclei are much higher, and the sensitivity of the compound nucleus decays to spin and parity is reduced. This is also true at higher energies: The competition between one- and two-neutron emission shows significant dependence on the compound-nuclear spins, although the sensitivity is not as strong as in the zirconium case. Figure 7 shows the one- and two-neutron emission probabilities for the ^{239}U nucleus. Like the gadolinium case discussed, the uranium nuclei are deformed and have a much higher level density than the zirconium nuclei: ^{238}U has 16 levels below 1 MeV. The transition from one-neutron to two-neutron emission, which lies near the threshold for second-chance fission, is also sensitive to the angular momentum population of the compound nucleus. Multiple channels compete at all energies considered and no clear plateaus for the probabilities emerge, unlike in the other cases considered.

For all three cases discussed, we have observed that there is enhanced sensitivity of the neutron emission probabilities near the thresholds. It can therefore be expected that a failure to account for the spin-parity mismatch in the analysis of surrogate reaction will result in extracted (n, n') and $(n, 2n)$ cross sections that do not reflect the true threshold behavior. This will be investigated in more detail in the next subsection.

B. Impact of spin dependence of $1n$ and $2n$ decay probabilities

In the previous section, we observed that the one- and two-neutron decay probabilities show a significant dependence on the spin of the compound nucleus and a lesser dependence on parity. Here we study the impact of this dependence on cross sections obtained under the assumption of the validity of the Weisskopf-Ewing approximation. We use the schematic spin distributions $F_\delta^{CN}(E_{ex}, J^\pi)$ discussed in Sec. III B 3. They are conveniently parametrized as discretized normal distributions with mean μ and variance $\sigma^2 = \mu$:

$$F_\delta^{CN}(E_{ex}, J^\pi) \propto \mathcal{N}(m = \mu, sd = \sqrt{\mu}). \quad (10)$$

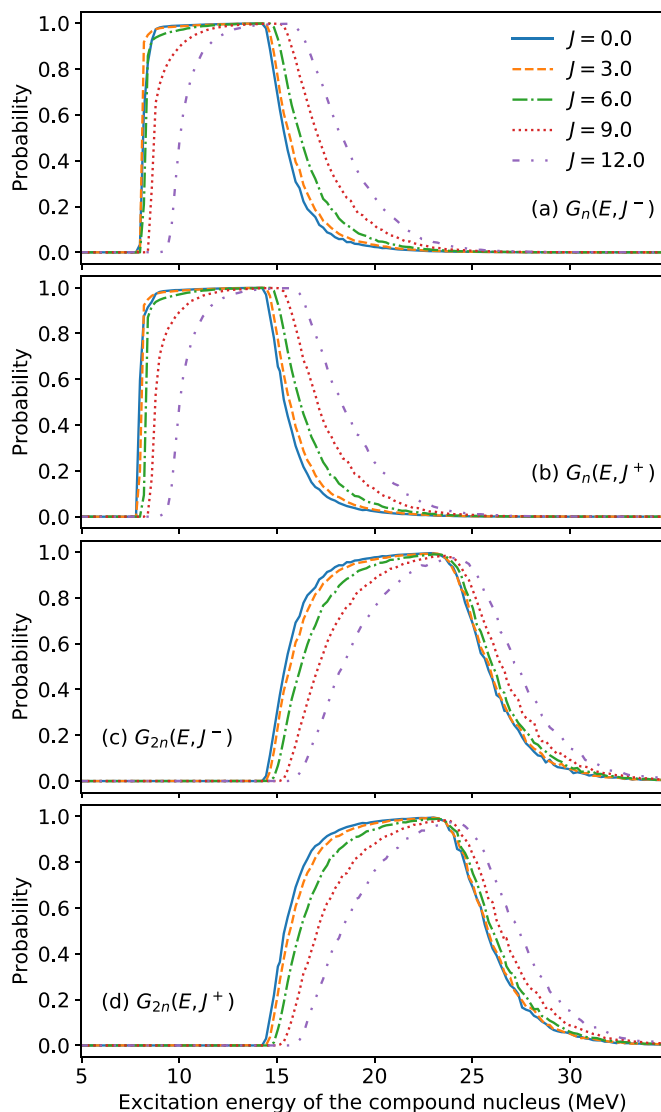


FIG. 6. Probabilities for one- and two-neutron emission from the $^{158}\text{Gd}^*$ nucleus, as functions of excitation energy, for various $J\pi$ values of the compound nucleus. The decay probabilities for both channels are seen to depend on the angular-momentum states populated in the compound nucleus, at the onset of one-neutron emission near $E_{ex} = S_n(^{158}\text{Gd}) = 7.937$ MeV and in the transition region where the two-neutron channel opens.

The distributions are cut off above $J = 50$ and normalized to unity. For the even-even compound nucleus $^{158}\text{Gd}^*$, we consider the five distributions $\mu = 1, 3, 5, 7, 9$, shown in Figure 4; for the odd nuclei $^{91}\text{Zr}^*$ and $^{239}\text{U}^*$ we use $\mu = 1.5, 3.5, 5.5, 7.5, \text{ and } 9.5$.

Results for $^{90}\text{Zr}(n, n')$ and $^{90}\text{Zr}(n, 2n)$ cross sections obtained from a Weisskopf-Ewing analysis of the simulated surrogate data are shown in Fig. 8. As expected, the threshold regions for both reactions are particularly sensitive to spin effects. At the onset of inelastic scattering, it is not possible to obtain a reliable (n, n') cross section; both shape and magnitude show a very large variance. Different spin distributions give the same magnitude of this cross section in the region

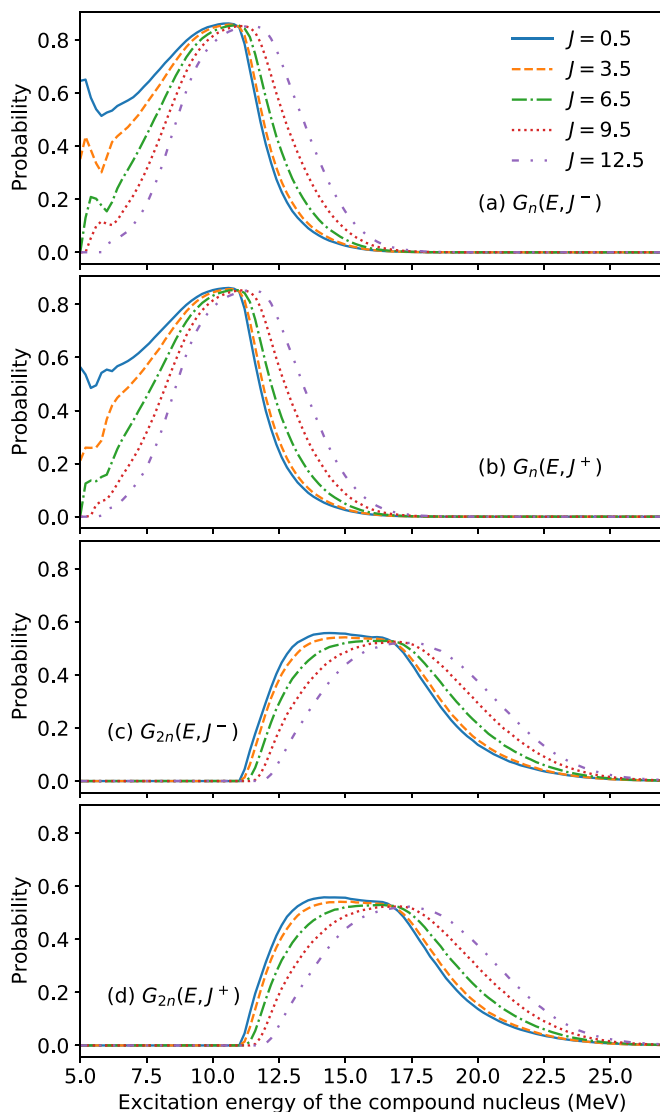


FIG. 7. Probabilities for one- and two-neutron emission from the $^{239}\text{U}^*$ nucleus, as function of excitation energy, for various $J\pi$ values of the compound nucleus. We observe a strong spin and parity dependence of $G_{1n}^{CN}(E_{ex}, J^\pi)$ near $E_{ex} = S_n(^{239}\text{U}) = 4.806$ MeV, which lies just below the threshold for fission.

of the plateau, but there is again significant uncertainty in the region where the two-neutron channel opens up.

Given the findings in the previous section, we expect the situation to be better for the gadolinium case, shown in Fig. 9. While the $^{157}\text{Gd}(n, n')$ cross section near the onset of inelastic scattering varies less than the analogous zirconium cross section, it is still quite unreliable. The value of the $^{157}\text{Gd}(n, n')$ cross section shows no dependence on the simulated spin-parity distribution in a region around $E_n = 5$ MeV. Not surprisingly, the Weisskopf-Ewing approximation for different sets of simulated surrogate data yields results that are consistent with each other in an energy regime where there is little to no competition from other decay channels. The maximum for the $^{157}\text{Gd}(n, 2n)$ cross section occurs near $E_n = 15$ MeV, where the different sets of surrogate data differ

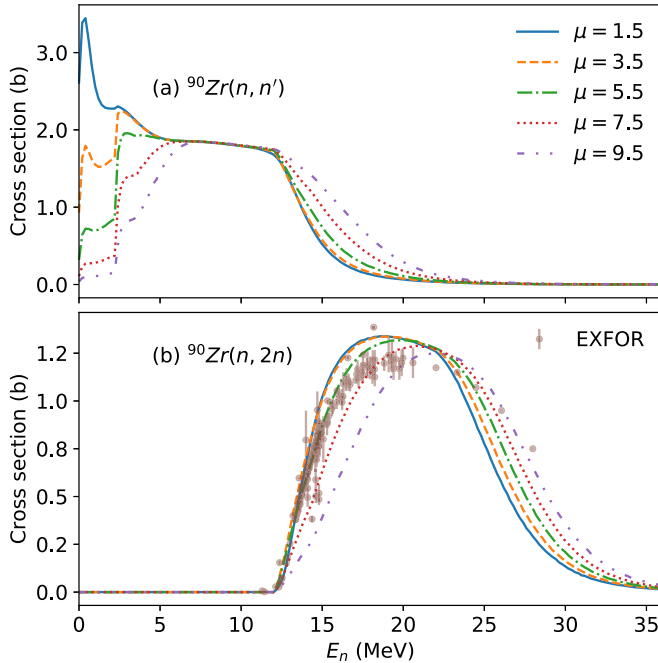


FIG. 8. Cross sections for (a) $^{90}\text{Zr}(n, n')$ and (b) $^{90}\text{Zr}(n, 2n)$, obtained from simulated surrogate data, using the Weisskopf-Ewing assumption. The underlying schematic spin-parity distributions used are indicated in the legend. The shape of the transition depends clearly on which simulated surrogate data is used, with the cross sections varying by $\pm 30\%$ at about $E_n = 15$ MeV. The $^{90}\text{Zr}(n, 2n)$ cross section varies by $\pm 4\%$ near its maximum, which is located at about $E_n = 20$ MeV. For comparison, experimental data [61] for $^{90}\text{Zr}(n, 2n)$ is shown in panel (b). The only data for the inelastic scattering case is for scattering to an isomeric state.

from each other by about 4%, which is an uncertainty that is similar to the error bands obtained from direct measurements. Overall, it appears that the Weisskopf-Ewing approximation might provide a very rough estimate of the $(n, 2n)$ cross section of a rare-earth nucleus.

For the uranium case, shown in Fig. 10, we observe a further decrease in sensitivity to differences in spin. Even so, the shape of the $^{238}\text{U}(n, n')$ cross section cannot be reliably extracted at low energies. With increasing energy, the Weisskopf-Ewing approximation appears to become more reliable. In fact, the $^{238}\text{U}(n, 2n)$ cross section obtained from the simulated data is in good agreement with available directly measured data. At energies above 18 MeV, however, where no data exist, we see deviations from the ENDF evaluation [36]. We attribute this to the neglect of pre-equilibrium contributions, which are included in evaluations but neglected in standard Weisskopf-Ewing analysis.

Overall, we find that the Weisskopf-Ewing approximation can provide rough first estimates for the $(n, 2n)$ cross sections of nuclei with large level densities, such as rare-earth and actinide nuclei, while the low-energy behavior is much less reliable. Specifically, near thresholds there is clearly increased sensitivity of the decay to the underlying spin-parity distribution in the compound nucleus. As a result, the shapes of the extracted cross sections do not reproduce the true cross sec-

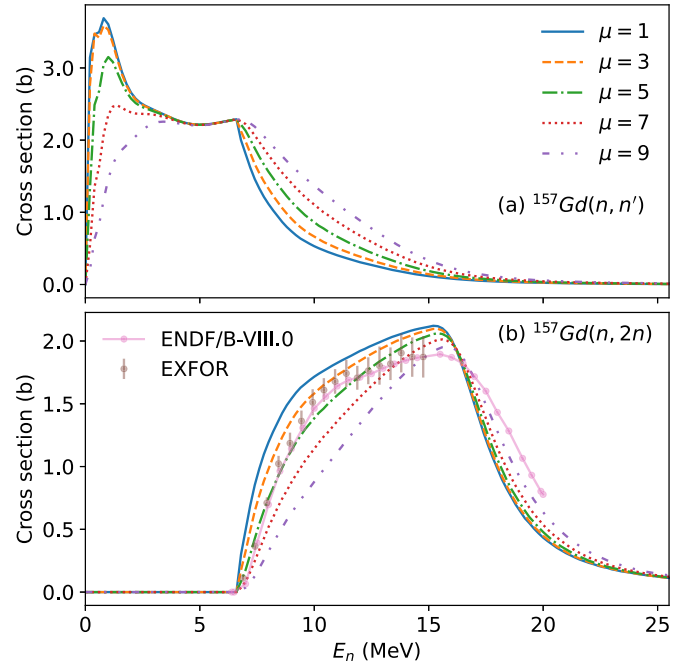


FIG. 9. Cross sections for $^{157}\text{Gd}(n, n')$ and $^{157}\text{Gd}(n, 2n)$, obtained from simulated surrogate data, using the Weisskopf-Ewing assumption and several schematic spin-parity distributions. In the energy region where the transition from one- to two-neutron emission occurs, the cross sections exhibit greater uncertainty, varying by $\pm 57\%$ for (n, n') and $\pm 13\%$ for $(n, 2n)$ at $E_n = 10$ MeV. The maximum for $(n, 2n)$ near $E_n = 15$ MeV, the variation is $\pm 62\%$ for (n, n') and $\pm 1\%$ for $(n, 2n)$. For comparison, directly measured data [61] is shown for the $^{157}\text{Gd}(n, 2n)$ cross section; no data are available for the inelastic cross section.

tions very well. Notably, the Weisskopf-Ewing approximation fails at the onset of one-neutron emission. This is in line with earlier findings about the limitations of this approximation for neutron capture cross sections.

In addition, it should be stressed that we have focused on the compound contributions to the (n, n') and $(n, 2n)$ cross sections here. For inelastic scattering, it is well known that direct (preequilibrium) mechanisms provide significant additional contributions, which are not considered here. These contributions are known to affect the spins populated in the target nucleus [62,63] and will exacerbate the deficiencies of the WE approximation. These have to be calculated separately and added to the cross section, similar to what is done for the direct-reaction component in an evaluation. Unfortunately, for many nuclei there is little data available for neutron inelastic scattering, and the calculations are challenging, so this reaction channel requires additional studies, both experimentally and theoretically.

V. OUTLOOK

We have investigated the potential use of the Weisskopf-Ewing approximation for determining (n, n') and $(n, 2n)$ cross sections from surrogate reaction data. Earlier work for neutron-induced fission and radiative neutron capture

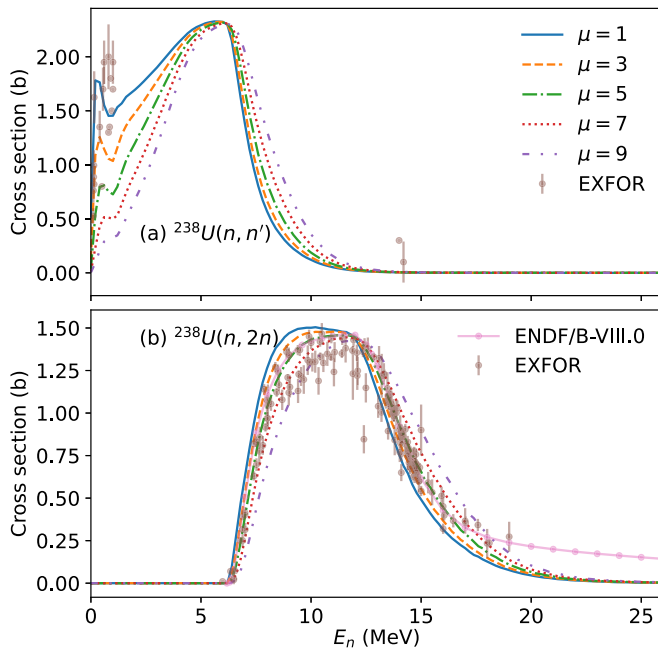


FIG. 10. Cross sections for (a) $^{238}\text{U}(n, n')$ and (b) $^{238}\text{U}(n, 2n)$, obtained from simulated surrogate data, using the Weisskopf-Ewing assumption and several schematic spin-parity distributions. The $^{238}\text{U}(n, 2n)$ results agree reasonably well with the existing data [61]. For the inelastic case, data are only available for low energies, where direct reaction mechanisms are known to contribute.

demonstrated that this approximation yields reasonable approximations for the fission cross sections, but fails for capture, making it necessary to employ more detailed theoretical modeling in the latter case.

We modeled the nuclear structure properties that determine the decay of a compound nucleus via $1n$ and $2n$ emission, as well as the combined effect of the nuclear structure and the surrogate reaction mechanisms on the cross-section results that one obtains from a Weisskopf-Ewing analysis of the indirect data. We found that the Weisskopf-Ewing approximation fails to give consistent cross section shapes in the presence of a spin-parity mismatch between the desired and surrogate reactions. The outcomes are worse for nuclei with low level density, i.e., for lighter nuclei and for those in regions near closed shells. While rough estimates for the cross sections might be obtained for $(n, 2n)$ reactions on well-deformed rare-earth and actinide nuclei, we find that nuclei in the mass-90 region are more sensitive to the effects of spin and parity. Furthermore, inelastic neutron scattering cross sections are found to be quite sensitive to angular-momentum effects and thus require a detailed treatment of the reaction mechanism, similar to that recently used for extracting capture cross sections from surrogate data.

Suggestions to find a surrogate reaction that approximates the spin-parity distribution relevant to the desired reaction are well motivated, as the use of the Weisskopf-Ewing approximation greatly simplifies surrogate applications. However, not enough is known about the angular momentum and parity of the compound states that are populated in a surrogate reaction

to plan an appropriate experiment. Recent work has demonstrated that the surrogate reactions that produce a compound nucleus at the high energies of interest involve higher-order reaction mechanisms, which render inadequate the type of simple angular-momentum estimates that are often used in traditional nuclear structure studies. It is also not necessarily true that a surrogate reaction produces spins in a compound nucleus that are higher than those relevant to neutron-induced reactions. This means that, in order to achieve cross section results with appropriate shapes and errors less than about 30%, surrogate reaction data will need to be combined with full modeling of the reaction mechanism, as described in Sec. II B.

In light of our findings that the Weisskopf-Ewing approximation is insufficient for determining (n, n') and $(n, 2n)$ cross sections, we believe that further development of surrogate reaction theory is important for addressing existing nuclear data needs. Inelastic scattering (n, n') reactions in particular are poorly constrained by direct measurement techniques. Alternative indirect methods [64] do not address (n, n') and $(n, 2n)$ reactions. Recent surrogate reaction applications to neutron capture have demonstrated how to proceed to accurately extract cross sections from surrogate data in situations where the Weisskopf-Ewing approximation fails [14,15,25]. Given the limited utility of the Weisskopf-Ewing approximation for neutron induced one- and two- neutron emission reactions, we conclude that additional developments are needed in order to describe the relevant reaction mechanisms, such as those involved in the $(^3\text{He}, ^3\text{He}')$ scattering experiment described in Fig. 1.

ACKNOWLEDGMENTS

This work was performed under the auspices of the U.S. Department of Energy by Lawrence Livermore National Laboratory under Contract No. DE-AC52-07NA27344 with support from LDRD Project No. 19-ERD-017, and the Defense Science and Technology Internship (DSTI) and Glenn T. Seaborg Institute (GTSI) summer student programs. A part of this work was supported by DOE Grant No. DE-FG02-03ER41272.

APPENDIX: CONDITIONS OF THE WEISSKOPF-EWING LIMIT

As discussed in Sec. II, if the decay probabilities $G_{\chi}^{\text{CN}}(E_{\text{ex}}, J^{\pi})$ are independent of spin and parity, or the surrogate reaction produces a compound-nucleus spin distribution which is very similar to that produced by the neutron-induced reaction, the cross section for the desired reaction can be obtained very simply as

$$\sigma_{n+A,\chi}(E_n) = \sigma_{n+A}^{\text{CN}}(E_{\text{ex}})P_{\delta\chi}^{\text{CN}}(E_{\text{ex}}), \quad (\text{A1})$$

where $P_{\delta\chi}^{\text{CN}}(E_{\text{ex}})$ is the coincidence probability determined from the surrogate measurement.

The latter of these options, the “serendipitous” or “matching” condition requires that $F_{\delta}^{\text{CN}}(J^{\pi}) \approx F_{n+A}^{\text{CN}}(E_{\text{ex}}, J^{\pi})$ holds. A comparison of $F_{n+A}^{\text{CN}}(E_{\text{ex}}, J^{\pi})$ for representative nuclei and energies E_{ex} , shown in Fig. 2 of this paper and in Fig. 3 of Ref. [27], with realistic surrogate spin-parity distributions,

such as those shown in Fig. 3, indicates that it is difficult to identify and carry out a surrogate reaction experiment that can achieve this condition.

Here, we briefly review the conditions in which the decay probabilities become approximately independent of J^π , i.e., $G_\chi^{CN}(E_{ex}, J^\pi) \rightarrow \mathcal{G}_\chi^{CN}(E_{ex})$ (see also Refs. [31,32]).

First, the energy of the compound nucleus has to be sufficiently high, so that almost all channels into which the nucleus can decay are dominated by integrals over the level density. In that case, the denominator in Eq. (2) does not include decays to discrete levels.

Second, correlations between the incident and outgoing reaction channels, which can be formally accounted for by including width fluctuation corrections [65], have to be negligible. These correlations enhance elastic scattering, at the expense of the inelastic and reaction cross sections, and are most prominent at the low energies relevant to capture reactions. Width fluctuations are negligible if the first condition (above) is satisfied.

Third, the transmission coefficients $T_{\chi'l_c j_c}^J$ associated with the available exit channels have to be independent of the spin of the states reached in these channels. This condition is sufficiently well satisfied since the dependence of transmission coefficients on target spin is very weak and, in fact, is ignored in many Hauser-Feshbach codes.

Fourth, the level densities ρ_{j_c} in the available channels have to be independent of parity and their dependence on the spin of the relevant nuclei has to be of the form $\rho_{j_c} \propto (2j_c + 1)$. While level densities are known to depend on parity, that dependence becomes weaker with increasing excitation energy and is often ignored in statistical reaction calculations. In addition, many successful applications use level densities that are parametrized in a form that is factorized (for each parity) as

$$\rho_{j_c}(U_C) = w(U_C) \frac{(2j_c + 1)}{2\sigma_C^2} \exp\left(\frac{-j_c(j_c + 1)}{2\sigma_C^2}\right), \quad (\text{A2})$$

where $w(U_C)$ contains the energy dependence of the level density and σ_C is the spin cutoff factor. At low energies ($E_{ex} \leq 3$ MeV), typical values for σ_C^2 are 7–10 in the Zr region and

12–16 in the Gd region [66]. As E_{ex} increases from a few MeV to about 20 MeV, σ_C^2 can increase by a factor 4 or more for these mass regions [59]. If we then assume that the spins populated in the residual nucleus are small compared to the σ_C , the level density can be written as

$$\rho_{j_c}(U_C) \approx \frac{w_C(U_C)}{2\sigma_C^2} (2j_c + 1). \quad (\text{A3})$$

When the above conditions are satisfied, the decay probabilities from Eq. (2) take the form

$$G_\chi^{CN}(E_{ex}, J^\pi) = \frac{\sum_{l_c j_c} \int T_{\chi'l_c j_c}^J w_C(U_C) (2j_c + 1) dE_\chi}{\sum_{\chi'l_c j_c} \int T_{\chi'l_c j_c}^J(E_{\chi'}) w_C(U_C') (2j_c' + 1) dE_{\chi'}}. \quad (\text{A4})$$

We can carry out the sum over j_c if we use the triangle rule $|j_\chi - j_c| < j_c < |j_\chi + j_c|$ to obtain the identity

$$\sum_{j_c} (2j_c + 1) = (2j_\chi + 1)(2j_c + 1),$$

and, analogously for the j_χ ,

$$\sum_{j_\chi} (2j_\chi + 1) = (2J + 1)(2l_c + 1),$$

to obtain the spin-independent decay probabilities

$$\mathcal{G}_\chi^{CN}(E_{ex}) = \frac{(\sum_{l_c} (2l_c + 1) T_{\chi'l_c}) \int (2j_c + 1) w_C(U_C) dE_\chi}{(\sum_{\chi'l_c} (2l_c + 1) T_{\chi'l_c}(E_{\chi'})) \int (2j_c' + 1) w_C(U_C') dE_{\chi'}}. \quad (\text{A5})$$

In summary, in order for the $G_\chi^{CN}(E_{ex}, J^\pi)$ to become independent of spin and parity, the energy E_{ex} of the compound nucleus must be high enough so that decays to the continuum of residual nuclei dominate, and the reaction must populate spins that are small relative to the spin cutoff parameter. Since neutron-induced reactions and surrogate reactions can produce different spin distributions, it is possible that the conditions for the validity of the Weisskopf-Ewing approximation are satisfied for one type of reaction, but not the other.

-
- [1] A. Arcones, D. W. Bardayan, T. C. Beers, L. A. Bernstein, J. C. Blackmon, B. Messer, B. A. Brown, E. F. Brown, C. R. Brune, A. E. Champagne, A. Chieffi, A. J. Couture, P. Danielewicz, R. Diehl, M. El-Eid, J. E. Escher, B. D. Fields, C. Fröhlich, F. Herwig, W. R. Hix *et al.*, White paper on nuclear astrophysics and low energy nuclear physics part 1: Nuclear astrophysics, *Prog. Part. Nucl. Phys.* **94**, 1 (2017).
- [2] A. C. Hayes, Applications of nuclear physics, *Rep. Prog. Phys.* **80**, 026301 (2017).
- [3] R. Capote, M. Herman, P. Obložinský, P. Young, S. Goriely, T. Belgya, A. Ignatyuk, A. Koning, S. Hilaire, V. Plujko, M. Avrigeanu, O. Bersillon, M. Chadwick, T. Fukahori, Z. Ge, Y. Han, S. Kailas, J. Kopecky, V. Maslov, G. Reffo *et al.*, RIPL - reference input parameter library for calculation of nuclear reactions and nuclear data evaluations, *Nucl. Data Sheets* **110**, 3107 (2009).
- [4] G. Baur and H. Rebel, Coulomb breakup of nuclei - applications to astrophysics, *Annu. Rev. Nucl. Part. Sci.* **46**, 321 (1996).
- [5] S. Typel and G. Baur, Theory of the Trojan-Horse method, *Ann. Phys. (NY)* **305**, 228 (2003).
- [6] J. E. Escher, J. T. Harke, F. S. Dietrich, N. D. Scielzo, I. J. Thompson, and W. Younes, Compound-nuclear reaction cross sections from surrogate measurements, *Rev. Mod. Phys.* **84**, 353 (2012).
- [7] A. Larsen, A. Spyrou, S. Liddick, and M. Guttormsen, Novel techniques for constraining neutron-capture rates relevant for r-process heavy-element nucleosynthesis, *Prog. Part. Nucl. Phys.* **107**, 69 (2019).
- [8] J. E. Escher, A. P. Tonchev, J. T. Burke, P. Bedrossian, R. J. Casperson, N. Cooper, R. O. Hughes, P. Humby, R. S. Ilieva, S. Ota, N. Pietralla, N. D. Scielzo, and V. Werner, Compound-nuclear reactions with unstable nuclei: Constraining theory

- through innovative experimental approaches, *EPJ Web Conf.* **122**, 12001 (2016).
- [9] W. Hauser and H. Feshbach, The inelastic scattering of neutrons, *Phys. Rev.* **87**, 366 (1952).
- [10] P. Fröbrich and R. Lipperheide, *Theory of Nuclear Reactions* (Clarendon, Oxford, 1996).
- [11] N. Scielzo (private communication).
- [12] R. O. Hughes, J. T. Burke, and J. E. Escher, Toward (n, n') and $(n, 2n)$ cross sections for ^{155}Gd using the surrogate reaction method and the NeutronSTARS detector, Lawrence Livermore National Laboratory, Technical Report No. LLNL-TR-839258 (2022).
- [13] V. Semkova, E. Bauge, A. Plompen, and D. Smith, Neutron activation cross sections for zirconium isotopes, *Nucl. Phys. A* **832**, 149 (2010).
- [14] J. E. Escher, J. T. Harke, R. O. Hughes, N. D. Scielzo, R. J. Casperson, S. Ota, H. I. Park, A. Saastamoinen, and T. J. Ross, Constraining Neutron Capture Cross Sections for Unstable Nuclei with Surrogate Reaction Data and Theory, *Phys. Rev. Lett.* **121**, 052501 (2018).
- [15] A. Ratkiewicz, J. A. Cizewski, J. E. Escher, G. Potel, J. T. Harke, R. J. Casperson, M. McCleskey, R. A. E. Austin, S. Burcher, R. O. Hughes, B. Manning, S. D. Pain, W. A. Peters, S. Rice, T. J. Ross, N. D. Scielzo, C. Shand, and K. Smith, Towards Neutron Capture on Exotic Nuclei: Demonstrating $(d, p\gamma)$ as a Surrogate Reaction for (n, γ) , *Phys. Rev. Lett.* **122**, 052502 (2019).
- [16] A. J. Koning and J.-P. Delaroche, Local and global nucleon optical models from 1 keV to 200 MeV, *Nucl. Phys. A* **713**, 231 (2003).
- [17] R. Varner, W. Thompson, T. McAbee, E. Ludwig, and T. Clegg, A global nucleon optical model potential, *Phys. Rep.* **201**, 57 (1991).
- [18] C. W. Johnson, K. D. Launey, N. Auerbach, S. Bacca, B. R. Barrett, C. R. Brune, M. A. Caprio, P. Descouvemont, W. H. Dickhoff, C. Elster, P. J. Fasano, K. Fosse, H. Hergert, M. Hjorth-Jensen, L. Hlophe, B. Hu, R. M. I. Betan, A. Idini, S. König, K. Kravvaris *et al.*, White paper: from bound states to the continuum, *J. Phys. G: Nucl. Part. Phys.* **47**, 123001 (2020).
- [19] C. D. Pruitt, J. E. Escher, and R. Rahman, Uncertainty-quantified phenomenological optical potentials for single-nucleon scattering, *Phys. Rev. C* **107**, 014602 (2023).
- [20] C. Hebborn, F. Nunes, G. P. Potel Aguilar, W. H. Dickhoff, J. W. Holt, M. C. Atkinson, R. B. Baker, C. Barbieri, G. Blanchon, M. Burrows, R. Capote Noy, P. Danielewicz, M. Dupuis, C. Elster, J. Escher, L. Hlophe, A. Idini, H. Jayatissa, B. P. Kay, K. Kravvaris *et al.*, Optical potentials for the rare-isotope beam era, *J. Phys. G: Nucl. Part. Phys.* (2023), doi: [10.1088/1361-6471/acc348](https://doi.org/10.1088/1361-6471/acc348).
- [21] W. Dickhoff and R. Charity, Recent developments for the optical model of nuclei, *Prog. Part. Nucl. Phys.* **105**, 252 (2019).
- [22] C. D. Pruitt, R. J. Charity, L. G. Sobotka, J. M. Elson, D. E. M. Hoff, K. W. Brown, M. C. Atkinson, W. H. Dickhoff, H. Y. Lee, M. Devlin, N. Fotiades, and S. Mosby, Isotopically resolved neutron total cross sections at intermediate energies, *Phys. Rev. C* **102**, 034601 (2020).
- [23] T. R. Whitehead, Y. Lim, and J. W. Holt, Global Microscopic Description of Nucleon-Nucleus Scattering with Quantified Uncertainties, *Phys. Rev. Lett.* **127**, 182502 (2021).
- [24] G. Blanchon, M. Dupuis, and H. F. Arellano, Prospective study on microscopic potential with Gogny interaction, *Eur. Phys. J. A* **51**, 165 (2015).
- [25] R. Pérez Sánchez, B. Jurado, V. Méot, O. Roig, M. Dupuis, O. Bouland, D. Denis-Petit, P. Marini, L. Mathieu, I. Tsekhanovich, M. Aïche, L. Audouin, C. Cannes, S. Czajkowski, S. Delpech, A. Görgen, M. Guttormsen, A. Henriques, G. Kessedjian, K. Nishio *et al.*, Simultaneous Determination of Neutron-Induced Fission and Radiative Capture Cross Sections from Decay Probabilities Obtained with a Surrogate Reaction, *Phys. Rev. Lett.* **125**, 122502 (2020).
- [26] S. Chiba and O. Iwamoto, Verification of the surrogate ratio method, *Phys. Rev. C* **81**, 044604 (2010).
- [27] J. E. Escher and F. S. Dietrich, Cross sections for neutron capture from surrogate measurements: An examination of Weisskopf-Ewing and ratio approximations, *Phys. Rev. C* **81**, 024612 (2010).
- [28] C. Forssén, F. S. Dietrich, J. Escher, R. D. Hoffman, and K. Kelley, Determining neutron capture cross sections via the surrogate reaction technique, *Phys. Rev. C* **75**, 055807 (2007).
- [29] W. Younes and H. C. Britt, Neutron-induced fission cross sections simulated from (t, pf) results, *Phys. Rev. C* **67**, 024610 (2003).
- [30] W. Younes and H. C. Britt, Simulated neutron-induced fission cross sections for various Pu, U, and Th isotopes, *Phys. Rev. C* **68**, 034610 (2003).
- [31] J. E. Escher and F. S. Dietrich, Determining (n, f) cross sections for actinide nuclei indirectly: Examination of the surrogate ratio method, *Phys. Rev. C* **74**, 054601 (2006).
- [32] E. Gadioli and P. E. Hodgson, *Pre-Equilibrium Nuclear Reactions* (Clarendon, Oxford, 1992).
- [33] A. J. Koning, S. Hilaire, and M. C. Duijvestijn, TALYS: Comprehensive nuclear reaction modeling, in *International Conference on Nuclear Data for Science and Technology, 26 September–1 October 2004, Santa Fe, New Mexico*, edited by R. C. Haight, M. B. Chadwick, T. Kawano, and P. Talou, AIP Conf. Proc. No. 769 (AIP, New York, 2005), p. 1154.
- [34] A. Koning, D. Rochman, J. Kopecky, J. C. Sublet, E. Bauge, S. Hilaire, P. Romain, B. Morillon, H. Duarte, S. van der Marck, S. Pomp, H. Sjostrand, R. Forrest, H. Henriksson, O. Cabellos, S. Goriely, J. Leppanen, H. Leeb, A. Plompen, and R. Mills, TENDL-2015: TENDL-based evaluated nuclear data library, https://tendl.web.psi.ch/tendl_2015/tendl2015.html.
- [35] W. Ormand, Monte Carlo Hauser-Feshbach computer code system to model nuclear reactions: YAHFC, Lawrence Livermore National Laboratory, Technical Report No. LLNL-TR-824700 (2021).
- [36] D. Brown, M. Chadwick, R. Capote, A. Kahler, A. Trkov, M. Herman, A. Sonzogni, Y. Danon, A. Carlson, M. Dunn, D. Smith, G. Hale, G. Arbanas, R. Arcilla, C. Bates, B. Beck, B. Becker, F. Brown, R. Casperson, J. Conlin *et al.*, ENDF/B-VIII.0: The 8th major release of the nuclear reaction data library with CIELO-project cross sections, new standards and thermal scattering data, *Nucl. Data Sheets* **148**, 1 (2018), Special Issue on Nuclear Reaction Data.
- [37] A. Koning and M. Duijvestijn, A global pre-equilibrium analysis from 7 to 200 MeV based on the optical model potential, *Nucl. Phys. A* **744**, 15 (2004).
- [38] M. Uhl and B. Strohmaier, STAPRE, A computer code for particle induced activation cross sections and related quantities,

- Institut für Radiumforschung und Kernphysik Technical Report No. IRK 76/01, rev. 1978 (unpublished).
- [39] G. Nobre, A. Palumbo, D. Brown, M. Herman, S. Hoblit, and F. Dietrich, Towards a coupled-channel optical potential for rare-earth nuclei, *Nucl. Data Sheets* **118**, 266 (2014).
- [40] G. P. A. Nobre, A. Palumbo, M. Herman, D. Brown, S. Hoblit, and F. S. Dietrich, Derivation of an optical potential for statically deformed rare-earth nuclei from a global spherical potential, *Phys. Rev. C* **91**, 024618 (2015).
- [41] E. S. Soukhovitskiĭ, R. Capote, J. M. Quesada, S. Chiba, and D. S. Martyanov, Nucleon scattering on actinides using a dispersive optical model with extended couplings, *Phys. Rev. C* **94**, 064605 (2016).
- [42] E. S. Soukhovitskiĭ, R. Capote, J. M. Quesada, S. Chiba, and D. S. Martyanov, Erratum: Nucleon scattering on actinides using a dispersive optical model with extended couplings [Phys. Rev. C 94, 064605 (2016)], *Phys. Rev. C* **102**, 059901(E) (2020).
- [43] V. Maslov, Y. Prodzinskij, N. Teterova, M. Baba, and A. Hasegawa, ^{238}U -nucleon-nucleus optical potential up to 200 MeV, *Nucl. Phys. A* **736**, 77 (2004).
- [44] F. S. Dietrich, I. J. Thompson, and T. Kawano, Target-state dependence of cross sections for reactions on statically deformed nuclei, *Phys. Rev. C* **85**, 044611 (2012).
- [45] G. Duhamel-Chrétien, G. Perrin, C. Perrin, V. Comparat, E. Gerlic, S. Galès, and C. P. Massolo, Neutron hole states in ^{89}Zr via the (\bar{p}, d) reaction at 58 MeV, *Phys. Rev. C* **43**, 1116 (1991).
- [46] J. E. Escher, T. Burke, J. Casperson, O. Hughes, and D. Scielzo, One-nucleon pickup reactions and compound-nuclear decays, *EPJ Web Conf.* **178**, 03002 (2018).
- [47] J. Lei and A. M. Moro, Reexamining closed-form formulae for inclusive breakup: Application to deuteron- and ^6Li -induced reactions, *Phys. Rev. C* **92**, 044616 (2015).
- [48] J. Lei and A. M. Moro, Numerical assessment of post-prior equivalence for inclusive breakup reactions, *Phys. Rev. C* **92**, 061602(R) (2015).
- [49] G. Potel, F. M. Nunes, and I. J. Thompson, Establishing a theory for deuteron-induced surrogate reactions, *Phys. Rev. C* **92**, 034611 (2015).
- [50] B. V. Carlson, R. Capote, and M. Sin, Inclusive proton emission spectra from deuteron breakup reactions, *Few-Body Syst.* **57**, 307 (2016).
- [51] G. Potel, G. Perdikakis, B. V. Carlson, M. C. Atkinson, W. Dickhoff, J. E. Escher, M. S. Hussein, J. Lei, W. Li, A. O. Macchiavelli, A. M. Moro, F. Nunes, S. D. Pain, and J. Rotureau, Toward a complete theory for predicting inclusive deuteron breakup away from stability, *Eur. Phys. J. A* **53**, 178 (2017).
- [52] N. D. Scielzo, J. E. Escher, J. M. Allmond, M. S. Basunia, C. W. Beausang, L. A. Bernstein, D. L. Bleuel, J. T. Harke, R. M. Clark, F. S. Dietrich, P. Fallon, J. Gibelin, B. L. Goldblum, S. R. Leshner, M. A. McMahan, E. B. Norman, L. Phair, E. Rodriguez-Vieitez, S. A. Sheets, I. J. Thompson *et al.*, Measurement of γ -emission branching ratios for $^{154,156,158}\text{Gd}$ compound nuclei: Tests of surrogate nuclear reaction approximations for (n, γ) cross sections, *Phys. Rev. C* **81**, 034608 (2010).
- [53] J. J. Ressler, J. T. Harke, J. E. Escher, C. T. Angell, M. S. Basunia, C. W. Beausang, L. A. Bernstein, D. L. Bleuel, R. J. Casperson, B. L. Goldblum, J. Gostic, R. Hatarik, R. Henderson, R. O. Hughes, J. Munson, L. W. Phair, T. J. Ross, N. D. Scielzo, E. Swanberg, I. J. Thompson *et al.*, Surrogate measurement of the $^{238}\text{Pu}(n, f)$ cross section, *Phys. Rev. C* **83**, 054610 (2011).
- [54] R. O. Hughes, C. W. Beausang, T. J. Ross, J. T. Harke, R. J. Casperson, N. Cooper, J. E. Escher, K. Gell, E. Good, P. Humby, M. McCleskey, A. Saastimoinen, T. D. Tarlow, and I. J. Thompson, $^{236}\text{Pu}(n, f)$, $^{237}\text{Pu}(n, f)$, and $^{238}\text{Pu}(n, f)$ cross sections deduced from (p, t) , (p, d) , and (p, p') surrogate reactions, *Phys. Rev. C* **90**, 014304 (2014).
- [55] S. Ota, J. T. Harke, R. J. Casperson, J. E. Escher, R. O. Hughes, J. J. Ressler, N. D. Scielzo, I. J. Thompson, R. A. E. Austin, B. Abromeit, N. J. Foley, E. McCleskey, M. McCleskey, H. I. Park, A. Saastamoinen, and T. J. Ross, Spin differences in the ^{90}Zr compound nucleus induced by (p, p') inelastic scattering and (p, d) and (p, t) transfer reactions, *Phys. Rev. C* **92**, 054603 (2015).
- [56] F. E. Bertrand, G. R. Satchler, D. J. Horen, J. R. Wu, A. D. Bacher, G. T. Emery, W. P. Jones, D. W. Miller, and A. van der Woude, Giant multipole resonances from inelastic scattering of 152-MeV alpha particles, *Phys. Rev. C* **22**, 1832 (1980).
- [57] R. Bonetti, L. Colombo, and K.-I. Kubo, Inelastic α -scattering to the continuum: A probe of α -clustering in nuclei, *Nucl. Phys. A* **420**, 109 (1984).
- [58] P. Martin, Y. Gaillard, P. de Saintignon, G. Perrin, J. Chauvin, G. Duhamel, and J. Loiseaux, Excitation of low-lying levels and giant resonances in ^{90}Zr via 57.5 MeV polarized proton inelastic scattering, *Nucl. Phys. A* **315**, 291 (1979).
- [59] T. von Egidy and D. Bucurescu, Experimental energy-dependent nuclear spin distributions, *Phys. Rev. C* **80**, 054310 (2009).
- [60] G. Boutoux, B. Jurado, V. Méot, O. Roig, L. Mathieu, M. Aïche, G. Barreau, N. Capellan, I. Companis, S. Czajkowski, K.-H. Schmidt, J. Burke, A. Bail, J. Daugas, T. Faul, P. Morel, N. Pillet, C. Théroine, X. Derkx, O. Sérot *et al.*, Study of the surrogate-reaction method applied to neutron-induced capture cross sections, *Phys. Lett. B* **712**, 319 (2012).
- [61] V. Zerkin and B. Pritychenko, The experimental nuclear reaction data (EXFOR): Extended computer database and web retrieval system, *Nucl. Instrum. Methods Phys. Res., Sect. A* **888**, 31 (2018).
- [62] D. Dashdorj, T. Kawano, P. E. Garrett, J. A. Becker, U. Agvaanluvsan, L. A. Bernstein, M. B. Chadwick, M. Devlin, N. Fotiadis, G. E. Mitchell, R. O. Nelson, and W. Younes, Effect of preequilibrium spin distribution on $^{48}\text{Ti} + n$ cross sections, *Phys. Rev. C* **75**, 054612 (2007).
- [63] M. Kerveno, M. Dupuis, A. Bacquias, F. Belloni, D. Bernard, C. Borcea, M. Boromiza, R. Capote, C. De Saint Jean, P. Dessagne, J. C. Drohé, G. Henning, S. Hilaire, T. Kawano, P. Leconte, N. Nankov, A. Negret, M. Nyman, A. Olacel, A. J. M. Plompen *et al.*, Measurement of $^{238}\text{U}(n, n'\gamma)$ cross section data and their impact on reaction models, *Phys. Rev. C* **104**, 044605 (2021).
- [64] A. C. Larsen, M. Guttormsen, M. Krtička, E. Běták, A. Bürger, A. Görger, H. T. Nyhus, J. Rekestad, A. Schiller, S. Siem, H. K. Toft, G. M. Tveten, A. V. Voinov, and K. Wikan, Analysis of possible systematic errors in the Oslo method, *Phys. Rev. C* **83**, 034315 (2011).
- [65] S. Hilaire, C. Lagrange, and A. J. Koning, Comparisons between various width fluctuation correction factors for compound nucleus reactions, *Ann. Phys. (NY)* **306**, 209 (2003).
- [66] T. von Egidy and D. Bucurescu, Spin distribution in low-energy nuclear level schemes, *Phys. Rev. C* **78**, 051301(R) (2008).